

PAPER • OPEN ACCESS

Frugal discrete memristive device based on potassium permanganate solution

To cite this article: Chetan C Revadekar *et al* 2021 *Mater. Res. Express* **8** 076304

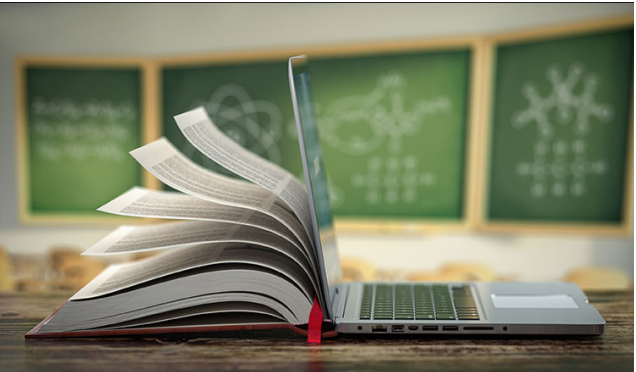
View the [article online](#) for updates and enhancements.



The Electrochemical Society
Advancing solid state & electrochemical science & technology
2021 Virtual Education

Fundamentals of Electrochemistry:
Basic Theory and Kinetic Methods
Instructed by: **Dr. James Noël**
Sun, Sept 19 & Mon, Sept 20 at 12h–15h ET

Register early and save!





PAPER

Frugal discrete memristive device based on potassium permanganate solution

OPEN ACCESS

RECEIVED

30 April 2021

REVISED

9 July 2021

ACCEPTED FOR PUBLICATION

15 July 2021

PUBLISHED

23 July 2021

Original content from this work may be used under the terms of the [Creative Commons Attribution 4.0 licence](#).

Any further distribution of this work must maintain attribution to the author(s) and the title of the work, journal citation and DOI.



Chetan C Revadekar^{1,5,*}, Ashkan Vakilipour Takaloo^{2,5}, Sandeep P Shinde³, Swapnil R Patil¹, Somnath S Kundale¹, Deok-kee Kim^{4,*}  and Tukaram D Dongale^{1,*} 

¹ Computational Electronics and Nanoscience Research Laboratory, School of Nanoscience and Biotechnology, Shivaji University, Kolhapur—416004, India

² School of Energy and Chemical Engineering, Ulsan National Institute of Science and Technology, Ulsan—44919, Republic of Korea

³ Department of Chemistry, Sathaye College, Vile Parle, Mumbai—400 057, India

⁴ Department of Electrical Engineering, Sejong University, 209 Neungdong-ro, Gwangjin-gu, Seoul—05006, Republic of Korea

⁵ Authors contributed equally to this work.

* Authors to whom any correspondence should be addressed.

E-mail: deokkeekim@sejong.ac.kr and tdd.snst@unishivaji.ac.in

Keywords: memristor, memristive switching, discrete device, volatile memory, electrochemistry, electrochemical impedance spectroscopy

Supplementary material for this article is available [online](#)

Abstract

Many thin film-based devices with solid electrolytes have been studied for memristive applications. Herein, we report a simple and facile way to fabricate solution-based, low-cost, and discrete two-terminal memristive devices using the KMnO_4 solution. The water and methanol were used as a solvent to prepare different concentrations of KMnO_4 to carry out the optimization study. Furthermore, the effect of KMnO_4 concentration with aqueous and methanol solvents was studied with the help of current-voltage, device charge, charge-flux, and cyclic endurance properties. Interestingly, all developed devices show the asymmetric time-domain charge and double valued charge-flux properties, suggesting that aqueous KMnO_4 and methanol- KMnO_4 based devices are non-ideal memristors or memristive devices. The statistical measures such as cumulative probability and coefficient of variation are reported for the memristive devices. The possible switching mechanism of the discrete memristive was tried to explain with the UV-visible spectrum and theoretical framework. The optimized device was further studied using the cyclic voltammogram, Bode plot, and Nyquist plot. An equivalent circuit was derived for the optimized discrete memristive device using electrochemical impedance spectroscopy results. The results of the present investigation are beneficial to develop programmable analog circuits, volatile memory, and synaptic devices using discrete memristive devices.

1. Introduction

In the existing passive device circuit family, the capacitor, inductor, and resistor are dominant fundamental elements governed by a basic set of variables such as current, charge, voltage, and magnetic flux. The prediction of a new fundamental circuit family member, named memristor was coined by Prof. Leon Chua in his influential research paper [1]. He argued with pairwise mathematical equations and correlated the charge and magnetic flux variables. In line with the theoretical prediction, an experimental realization of a solid-state memristor was achieved by HP researchers based on the resistive switching (RS) effect [2]. The memory with resistance property of memristor catches the eye of material physicists, device engineers, and application developers for better and efficient devices for memory [3, 4], synaptic computation [5, 6], sensing [7, 8], and image processing applications [9, 10]. However, the so-called ideal properties of the memristor, as described in the 1971 paper, are very hard to get in experimental ways [11]. On the other hand, the non-ideal memristor devices which having few ideal memristor properties but unable to demonstrate every property are becoming the cornerstone for

many applications [12–15]. These non-ideal memristors or more generally called memristive devices are possessed memory and nonlinearity properties that can be exploited for practical applications [16–18].

In practice, the memristive phenomenon is studied with the help of a sandwich structure consisting of a metal-switching layer-metal. For instance, Pt/oxide/Pt [19], Au/polymer/ITO [20], Au/DNA/Au [21], Ag/cellulose-fibers/Al [22], Ag/melanin/SS [23], Au/perovskite/FTO [24], and Ag/ferrite/FTO [25] are popular device configurations for the development of functional memristive devices. Few attempts have been dedicated to realized solid-state discrete memristive devices by utilizing the metal-semiconductor point contact [26], ZnO-rGO composite [27], and ZnO nanowires [28]. The active switching layer of conventional memristive devices is in the form of solid electrolytes, sandwiched between two metal electrodes. Apart from solid electrolytes, soft materials are getting attention in recent years owing to their solution processability and low cost [29]. The ionic transport is a key feature of soft material-based memristive devices. Interestingly, biological neurons and synapses are also working on the ionic transportation principle [29]. In addition to this, the memristive and RS effect was also observed in some liquid systems [30, 31]. Considering the usefulness of liquid-based devices, some research groups have mimicked the synaptic functionalities using liquid-based memristive devices [32, 33]. Apart from this, discrete mem-devices are useful to develop analog and digital electronic circuits with improved functionalities.

In the present work, a new two-terminal, discrete, and low-cost memristive device was developed using aqueous (aq.) potassium permanganate (KMnO_4) solution and KMnO_4 in methanol solution. The proposed discrete memristive devices show the fingerprint memristive hysteresis loop. The optimization study was carried out by varying the molar concentrations of aq. (KMnO_4) and KMnO_4 in methanol solutions. The memristive device containing 0.75 M aq. KMnO_4 shows the superior memristive property, consistent endurance, and a good memory window (~ 124). The possible switching mechanism of the discrete memristive device was reported and the optimized device was further studied by using cyclic voltammogram (CV), Bode plot, and Nyquist plot. An equivalent circuit was derived for the optimized device using electrochemical impedance spectroscopy (EIS) results.

2. Experimental details

2.1. Materials and methodology

The analytical grade KMnO_4 (Thomas Baker, Mumbai, India) was further used to prepare different molar concentrations in water and methanol solvents to develop discrete memristive devices. Different molar solutions of KMnO_4 such as 0.75 M, 0.50 M, 0.25 M, 0.1 M, 0.01 M, 0.001 M, and 0.0001 M were prepared by using deionized water having conductivity $\sim 0.5 \mu\text{S cm}^{-1}$ and methanol (99%, analytical Grade) procured from Thomas Baker, Mumbai, India.

2.2. Development of discrete devices and characterizations

The measurement setup to investigate the memristive properties of the discrete device containing KMnO_4 solutions is shown in figure 1. The laboratory-grade sample tubes and copper electrodes were used for the development of discrete devices. Before making the discrete devices, the sample tubes were cleaned with deionized water and dried overnight to remove all traces of water. For this work, thin and thick electrodes having diameters 2.05 mm and 1.048 mm respectively were used to make the device. The device was made up of two same-sized electrodes (symmetric electrodes) and with different sized electrodes (asymmetric electrodes) (thick: 2.05 mm–2.05 mm; thin: 1.048 mm–1.048 mm) and an asymmetric diameter sized (2.05 mm–1.048 mm) copper electrodes combinations were used to develop the discrete devices. The copper rods (act as electrodes) were inserted in the tube, such a way that the distance between two electrodes was 1 cm and both copper rods were placed at 1 cm deep in the sample tube, as shown in figure 1. The Bondtite was used for the effective sealing of copper electrodes with the tube to avoid the leakage of the KMnO_4 solution from the devices. For electrical measurements, the positive and negative terminals were connected to the symmetric thick copper electrode having diameter size (2.05 mm – 2.05 mm) or to the symmetric thin copper electrode having diameter size (1.048 mm – 1.048 mm) by filling the tube with aq. and KMnO_4 in methanol solutions. In the case of electrical measurements by using asymmetric electrodes, the thick electrode (2.05 mm) and thin electrode (1.048 mm) were connected to positive and negative terminals, respectively.

The current-voltage (I - V) and endurance measurements were carried out by using a memristor characterization system (ArC ONE). The optical spectrum was recorded using a UV–visible spectrophotometer (Cary-60, Agilent Technology). For this, aq. KMnO_4 solution was transferred from a laboratory-grade tube to a standard cuvette (1 cm) after applying the switching voltage. The UV–vis measurements were recorded in the wavelength range of 200 nm to 800 nm. The electrochemical workstation (Autolab N-Series) was used for the measurements of the CV, Bode plot, Nyquist plot, and EIS. The electrochemical measurements were carried out

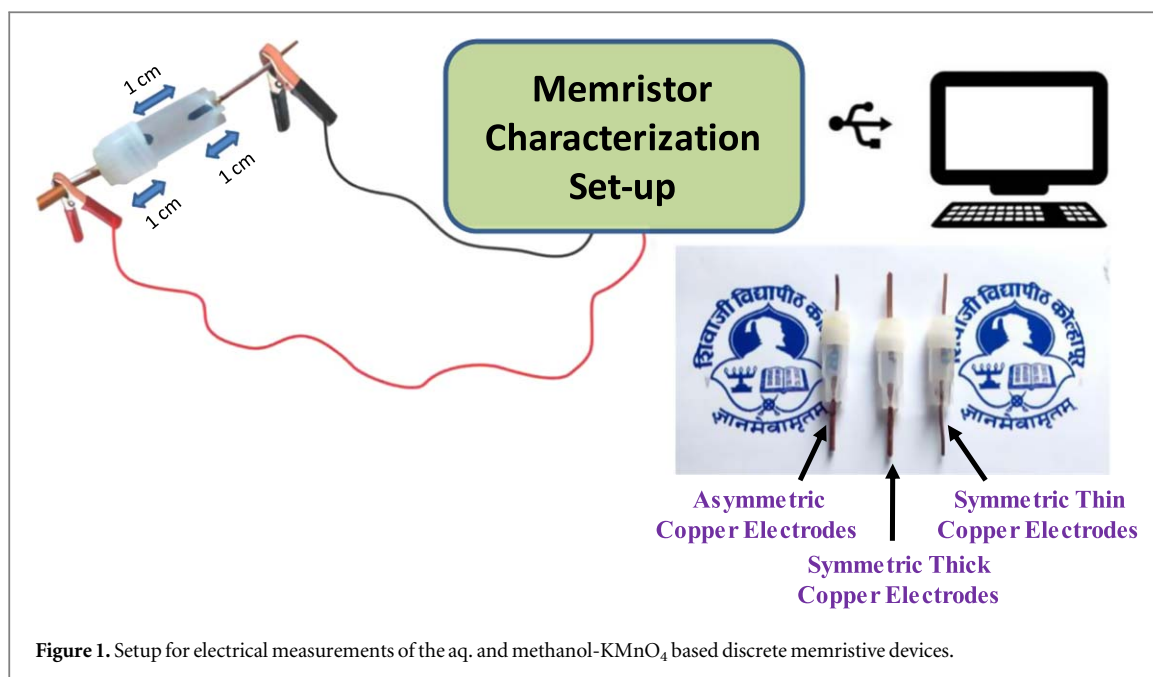


Figure 1. Setup for electrical measurements of the aq. and methanol-KMnO₄ based discrete memristive devices.

using the two-electrode system (Cu-Cu), as per Song *et al* report [34]. In particular, the reference and counter electrodes were sorted in one electrode and connected to one of the terminals. The working electrode was connected to the opposite terminal. The EIS study was carried out at a signal amplitude of 10 mV_{AC} and the sweeping frequency range was 1 Hz to 1 MHz.

3. Results and discussions

Recently, memristor/memristive devices have been attracted much attention from academia and industry due to their broad applications in resistive memory, brain-inspired computing, and reconfigurable circuits [35]. *I-V* hysteresis loop is an essential criterion for a device to be a memristor/memristive device [36, 37]. Recently, the RS effect was correlated with memristive switching [38]. In this work, we have fabricated discrete memristive devices using low lost synthesis techniques and demonstrated the volatile memory and electrochemical properties of the same. For this, we have used aq. KMnO₄ and KMnO₄ in methanol as a model material and developed devices with different concentrations (molar) of KMnO₄ for optimization study. *I-V* hysteresis curves of concentration-dependent aq. KMnO₄ based discrete devices with different electrode configurations and corresponding memristive areas are shown in figure 2. *I-V* characteristic was measured for different molar concentrations of aq. KMnO₄ solutions with different combinations of copper electrodes such as asymmetric, symmetric thick, and symmetric thin electrodes. For all *I-V* measurements, ±1 V amplitude and 2 ms step width-based staircase signals were used. *I-V* curves show a hysteresis loop with non-zero crossing property, as shown in figure S1 (supporting information available online at stacks.iop.org/MRX/8/076304/mmedia). The hysteresis loop and non-zero crossing properties confirm the memristive nature of the developed devices [39]. A transition from high resistance state (HRS) to low resistance state (LRS), generally known as the SET process has occurred at +1 V. As the voltage swept direction changed from 1 V to -1 V, the devices hold the LRS until the -1 V switching point. The devices shift the resistance state from LRS to HRS (RESET process) at -1 V and retain it in the -1 V to 0 V bias range. The diverse nature of hysteresis loops and current magnitudes were observed for asymmetric, symmetric thick, and symmetric thin copper electrode-based devices. Furthermore, concentration-dependent *I-V* switching was observed for the aq. KMnO₄ based discrete devices. From the *I-V* curves, it is observed that the device containing symmetric thick copper electrodes (figure 2(b)) shows comparable higher hysteresis loops and current magnitude than the device containing asymmetric copper electrodes (figure 2(a)) and symmetric thin copper electrodes (figure 2(c)). In addition to this, the memristive hysteresis area and current magnitude were tended to decreases as the concentration of aq. KMnO₄ decreases, as shown in figure 2(d).

Interestingly, all devices show the analog switching property in which current gradually increases or decreases under the influence of the external voltage. The aq. KMnO₄ based memristive devices resemble the properties of biological neurons and synapses in many ways such as the analog switching property (synaptic weight), two-terminal device structure (pre-and post-synaptic terminals), ionic transportation (synaptic cleft),

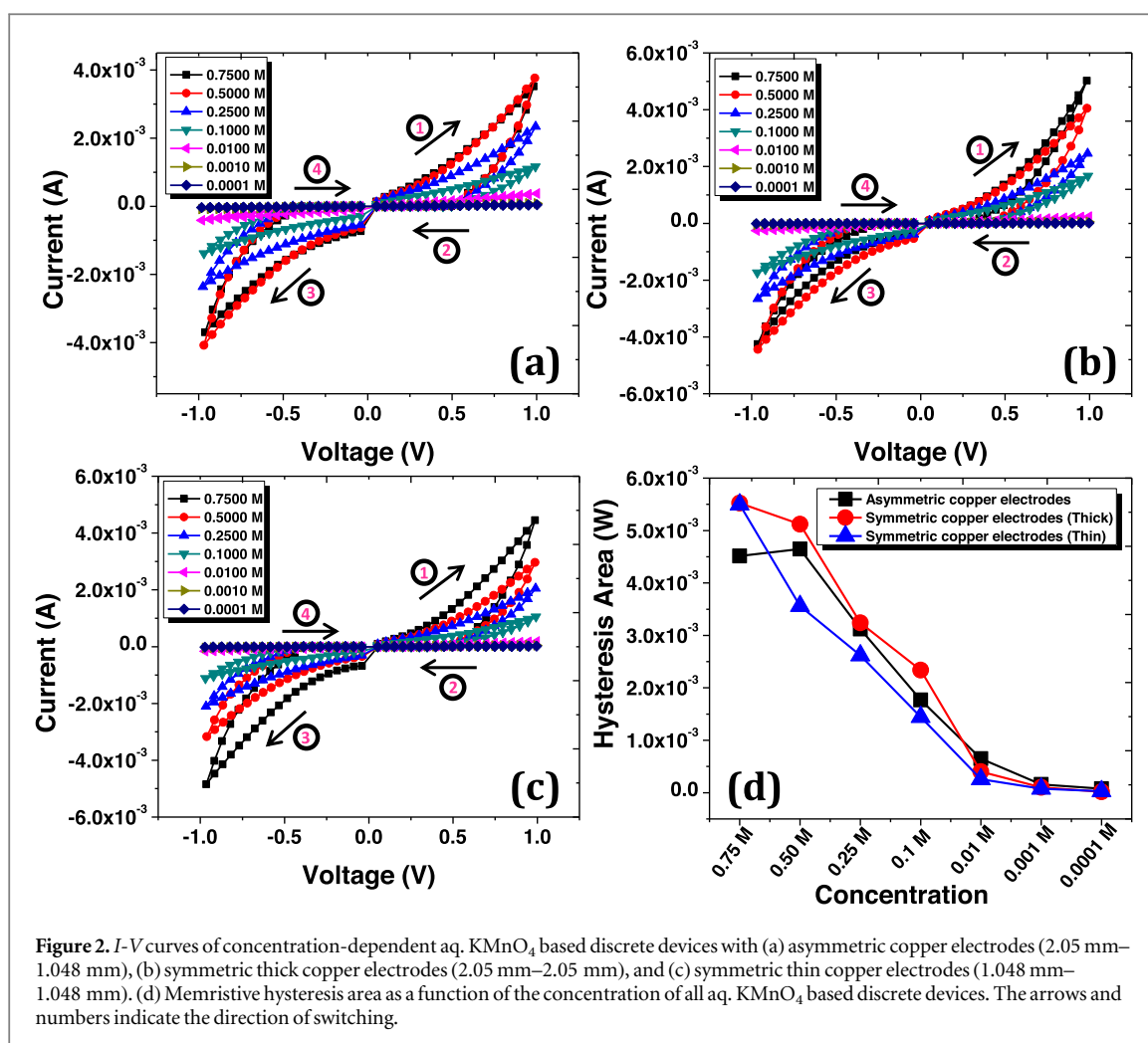


Figure 2. *I-V* curves of concentration-dependent aq. KMnO₄ based discrete devices with (a) asymmetric copper electrodes (2.05 mm–1.048 mm), (b) symmetric thick copper electrodes (2.05 mm–2.05 mm), and (c) symmetric thin copper electrodes (1.048 mm–1.048 mm). (d) Memristive hysteresis area as a function of the concentration of all aq. KMnO₄ based discrete devices. The arrows and numbers indicate the direction of switching.

and concentration-dependent *I-V* switching (depression) [40]. In the case of the biological neuron and synapse, memory and learning are achieved by the strength (synaptic weight) and occurrence of signals from the pre- to post-synaptic terminal [41]. The observed properties can be used for the development of discrete analog memory devices and can play a potential role in developing liquid electronic synaptic devices that mimic functionalities of the biological synapse.

In the next stage of work, methanol was used instead of deionized water to investigate the solvent effect on the KMnO₄ based discrete devices. Similar to the aq. KMnO₄ based discrete devices, the concentrations of the KMnO₄ in methanol such as 0.75 M, 0.50 M, 0.25 M, 0.1 M, 0.01 M, 0.001 M, and 0.0001 M were prepared and used in devices. Furthermore, the thickness of copper electrodes was also varied to investigate the symmetric and asymmetric chemical reactions. Figure 3 depicts the *I-V* traces of KMnO₄ in methanol solution-based discrete devices with different concentrations and different thicknesses of copper electrodes. On a similar line of the aq. KMnO₄ based discrete devices, the KMnO₄ in methanol-based discrete devices show the bipolar RS, analog switching, and memristive properties. However, the strict concentration-dependent *I-V* switching was not observed for asymmetric, symmetric thick, and symmetric thin copper electrode-based discrete devices containing KMnO₄ in methanol solutions, as shown in figures 3(a)–(c), respectively. In particular, the *I-V* traces were showed the different magnitude of the current with respect to the concentration variation in each device configuration. Furthermore, the memristive hysteresis area was not displaying the linear dependency on the concentration, as shown in figure 3(d). This kind of non-linearity is not acceptable for any practical application.

The pinched hysteresis loop in the current-voltage (*I-V*) plane is the fingerprint characteristic of the ideal memristor [39]. In general, the ideal memristor shows a type I hysteresis loop [42], in which *I-V* curves crosses at the origin. In certain cases, the ideal properties of the memristor are not observed and devices show the non-zero *I-V* crossings and double valued $q-\phi$ relation. Therefore, these non-ideal devices are referred to as extended memristor or memristive devices. In the literature, various non-ideal memristor or memristive devices have been reported [43–46]. However, the hysteresis loop cannot be the sole criterion to categorize the developed device as an ideal memristor or a non-ideal memristor (memristive) device. The theoretical description of the ideal memristor suggested that the device should have a non-linear and single-valued charge-magnetic flux

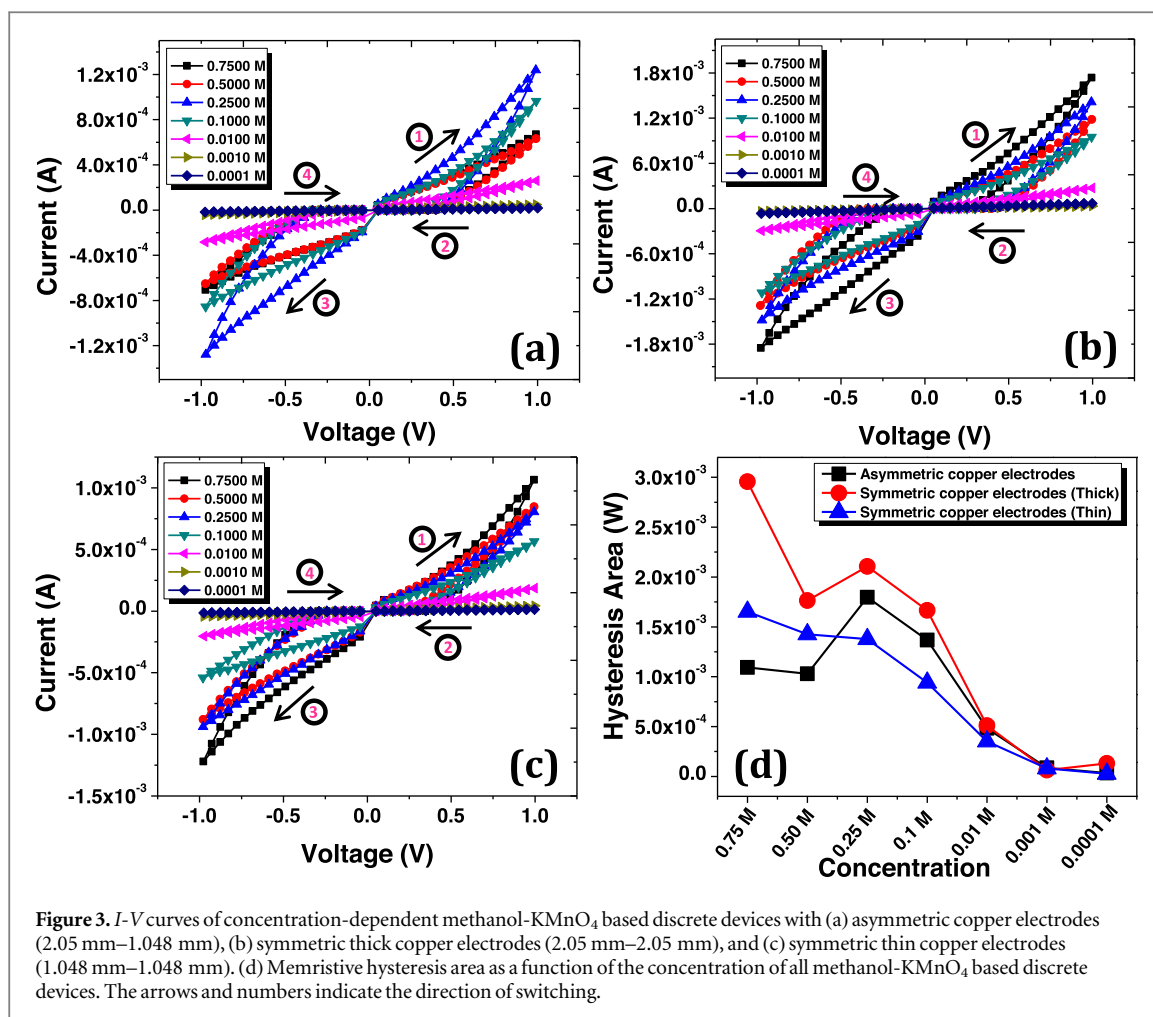
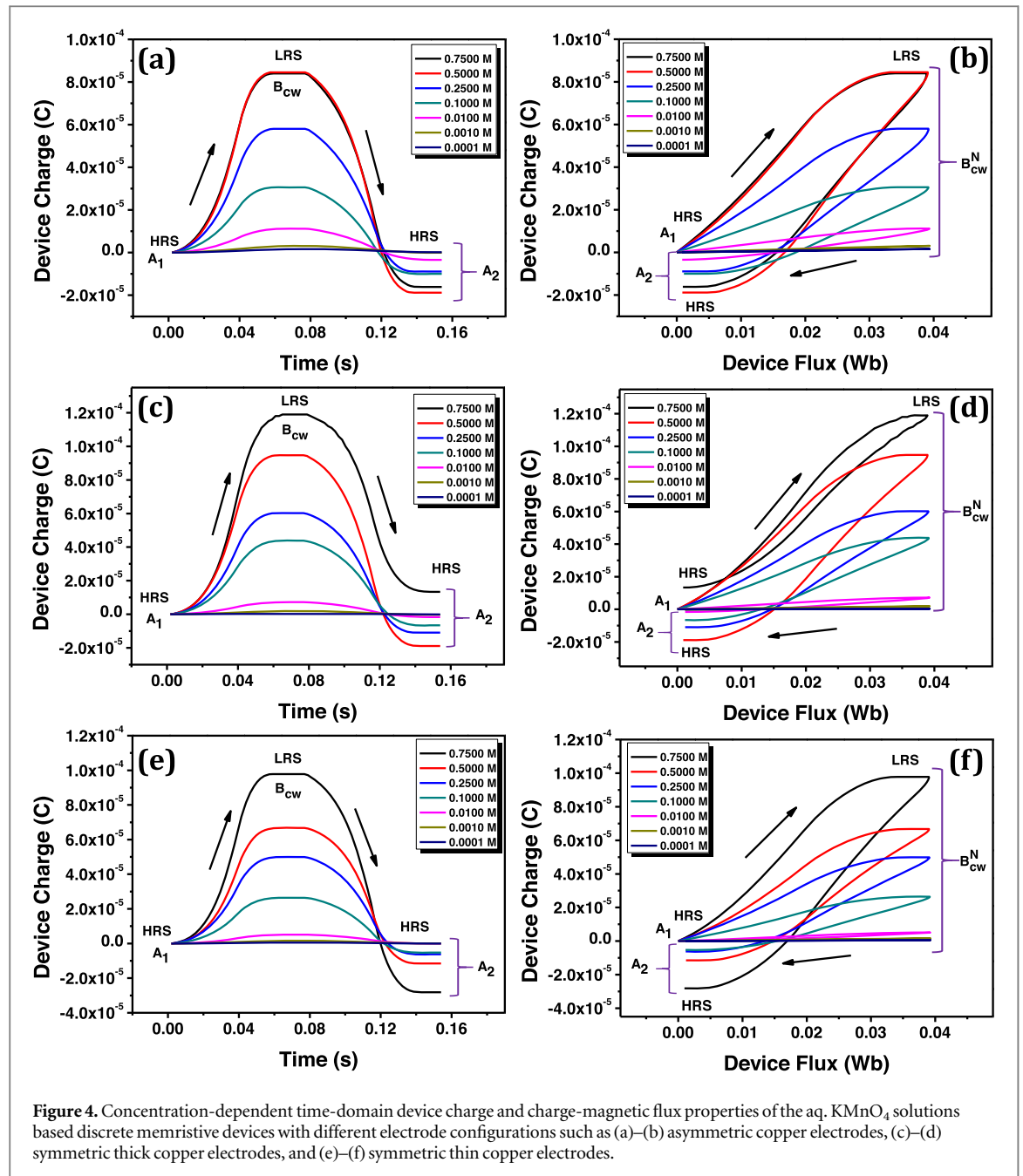


Figure 3. *I-V* curves of concentration-dependent methanol-KMnO₄ based discrete devices with (a) asymmetric copper electrodes (2.05 mm–1.048 mm), (b) symmetric thick copper electrodes (2.05 mm–2.05 mm), and (c) symmetric thin copper electrodes (1.048 mm–1.048 mm). (d) Memristive hysteresis area as a function of the concentration of all methanol-KMnO₄ based discrete devices. The arrows and numbers indicate the direction of switching.

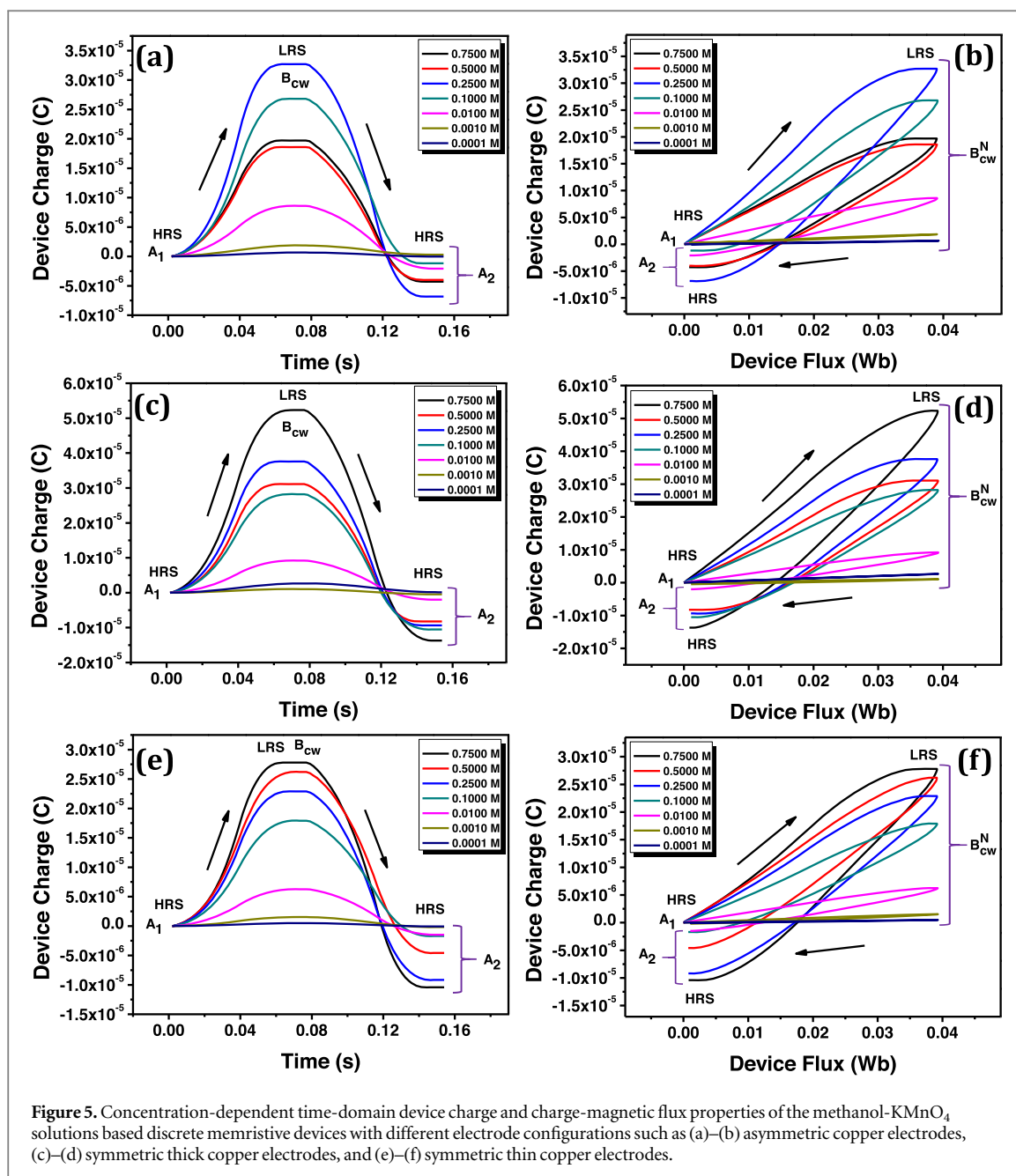
property [1]. However, many practical devices can deviate from the theoretical description of memristor [47–50]. The single-valued charge-magnetic flux test was used in the present investigation to show that the fabricated devices were non-ideal memristors. For the calculation of memristive properties, we have utilized a well-known correlation between charge-current and flux-voltage [51]. The fundamental circuit variables (current, voltage, charge, and magnetic flux) have symmetric relations with circuit elements (resistor, capacitor, inductor, and memristor). Therefore, current and voltage are related to the device charge and magnetic flux, respectively [37]. We have calculated charge and magnetic flux based on the mathematical formulation reported in the ref. [51]. The $q-\varphi$ curve depends on the shape, amplitude, number of measurement points, and time per measurement point of the input signal [51]. The calculated charge and magnetic flux are combined to find out the charge-magnetic flux nature of the device. Furthermore, we have combined them to find out the charge-magnetic flux nature of the device. Various interesting variables such as initial (A_1), half-period (B_{CW}), final-period (A_2), and turning points (B_{CW}^N) were observed from the calculated data.

The calculated device charge and charge-magnetic flux properties of the aq. and methanol-KMnO₄ based discrete devices with different electrode configurations and concentrations are shown in figures 4(a)–(f) and 5(a)–(f), respectively. The concentration-dependent time-domain flux characteristics of all devices with different electrode configurations are shown in figure S2 (supporting information). The time-domain flux characteristic of all devices is symmetrical due to the application of the symmetric voltage (± 1 V) to both devices irrespective of the device configuration. However, a highly asymmetrical device charge characteristic was observed for the aqueous and methanol-KMnO₄ based discrete devices. For the aqueous KMnO₄ based discrete devices, the time domain device charge varies as a function of the concentration. In particular, half period and final period points were varied proportional to the concentration, as shown in figures 4(a), (c), and (e). Similar to the time domain device charge, the charge-flux property of the aq. KMnO₄ based devices show the concentration-dependent device charge, half period, and final period points, as shown in figures 4(b), (d), and (f). However, no correlation was observed between device charge, half period, and final period concerning the concentration variation in the case of methanol-KMnO₄ based devices, as shown in figures 5(a), (c), and (e). A similar kind of trend was observed for the device charge-flux characteristic of methanol-KMnO₄ based devices, as shown in figures 5(b), (d), and (f). The detailed concentration-dependent final-period and turning points of



both devices are shown in figure S3 (supporting information). Interestingly, aq. and methanol- KMnO_4 based discrete devices show the double valued charge-flux property irrespective of the device configurations. This suggested that the aqueous and methanol- KMnO_4 based discrete devices are non-ideal memristors or memristive devices.

In the case of the methanol- KMnO_4 based discrete memristive devices, the symmetric thick electrode-based devices show a higher magnitude of current, good memristive switching, and hysteresis area similar to the aq. KMnO_4 based counterpart. Given this, the symmetric thick electrode-based aq. and methanol- KMnO_4 based discrete memristive devices were used for further memory characterizations and statistical analysis. The devices were subjected to the 10^3 switching cycles to test the cyclic endurance and memory properties of the KMnO_4 based discrete memristive devices. Furthermore, cumulative probability, coefficient of variation, and memory window of the LRS and HRS were determined by using temporal switching events. The alternative cyclic (AC) endurance property of an optimized 0.75 M KMnO_4 based discrete memristive device is shown in figure 6(a). The test conditions are as follows- write voltage: ± 1 V, read voltage: 0.25 V, pulse width: 500 μs . The endurance measurement of optimized devices shows two-level switching between LRS and HRS for consecutive 10^3 switching cycles. No usual deprivation in the switching events was observed. This confirms the reliability of the discrete memristive devices. It was observed that aq. KMnO_4 based memristive device shows lower LRS and



higher HRS values than methanol-KMnO₄ based counterpart. The switching uniformity of LRS and HRS was determined by calculating the cumulative probability of the switching events, as shown in figure 6(b). The LRS of both devices possesses good switching uniformity whereas, non-uniformity was observed for the HRS. In particular, highly non-uniformity switching probability was observed for the HRS of the aq. KMnO₄ based memristive device.

To determine the quantifiable variation in the switching events, the coefficient of variation was calculated for symmetric thick electrode-based aq. and methanol-KMnO₄ based discrete memristive devices. The concentration-dependent coefficient of variation is summarized in figure 6(c). The coefficient of variation of both devices was non-linearly increased and decreased as a function of concentration. In particular, the LRS of both devices shows a lower coefficient of variation values as compared to the HRS. A higher coefficient of variation values was observed for the HRS of the aq. KMnO₄ based discrete memristive device, whereas, HRS of the methanol-KMnO₄ based discrete memristive device shows a moderate coefficient of variation values. The coefficient of variation of LRS and HRS is not greater than 12%, indicating the good temporal switching uniformity of the developed memristive devices. The switching uniformity of developed discrete memristive devices is better than a few solid electrolytes-based memristive/RS devices [52–54]. The ratio of HRS and LRS is

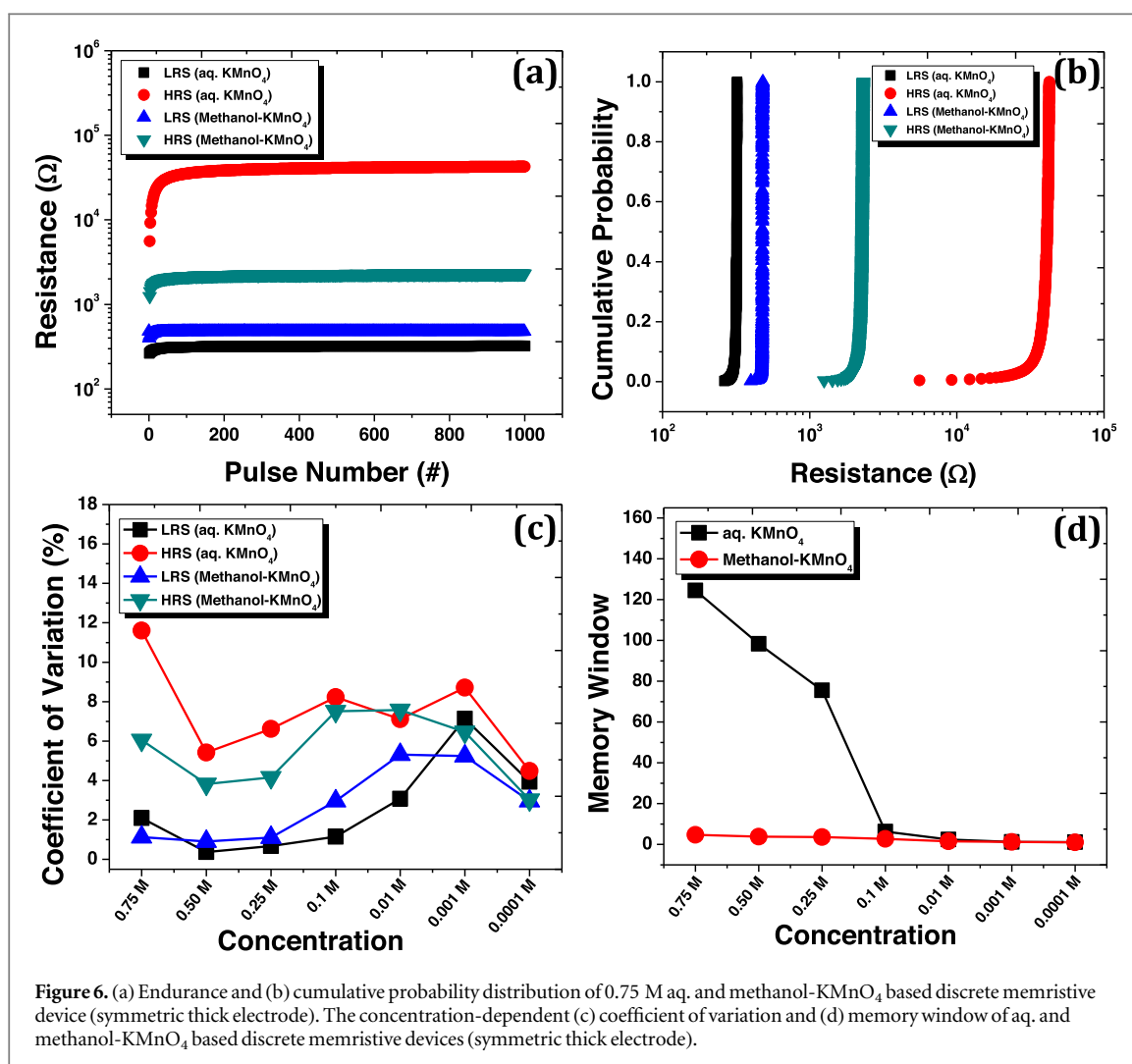


Figure 6. (a) Endurance and (b) cumulative probability distribution of 0.75 M aq. and methanol-KMnO₄ based discrete memristive device (symmetric thick electrode). The concentration-dependent (c) coefficient of variation and (d) memory window of aq. and methanol-KMnO₄ based discrete memristive devices (symmetric thick electrode).

considered as a memory window of the memristive device, and it should be high (>10) for practical applications to measure the errorless resistance state of the device [55].

The concentration-dependent memory window (for symmetric thick electrode) of aq. and methanol-KMnO₄ based discrete memristive devices are shown in figure 6(d). In the present case, the memory window tends to decrease as a function of the concentration. However, a good memory window was observed for the aq. KMnO₄ based memristive devices at higher concentrations and decreases for lower concentration. The excellent memory window (~ 124) was achieved for 0.75 M based aq. KMnO₄ device whereas methanol-based devices show a lower memory window (< 5) for all concentrations. The proposed discrete memristive devices did not show resistance retention as a function of time. Therefore, these devices behaved as volatile resistive switches. The statistical calculation suggested that the 0.75 M based aq. KMnO₄ memristive device has a good memory window; therefore, switching mechanisms and electrochemical characterizations studies were carried out for the same. In the case of optimized Cu/Aq. KMnO₄ (0.75 M)/Cu memristive device, the bipolar RS effect was induced by applying external electrical potential and switching was occurred due to ion migration from one electrode to another due to the influence of electrical potential.

The possible memristive switching phenomenon of the aq. KMnO₄ based discrete device is explained based on ionic conduction of manganese and copper ions, as shown in figure 7. The aq. KMnO₄ solution acts as an oxidizing agent, so this oxidizes the copper electrode at the electrode-electrolyte interface. When KMnO₄ is dissolved in distilled water, it gets dissociated into K⁺ and MnO₄⁻ ions. When the potential was applied across the two electrodes of the device, the following reactions took place:

Anode: Cu electrode; oxidation of Cu electrode in the presence of aq. KMnO₄ results in the following redox reaction,



(Oxidation due to external voltage)

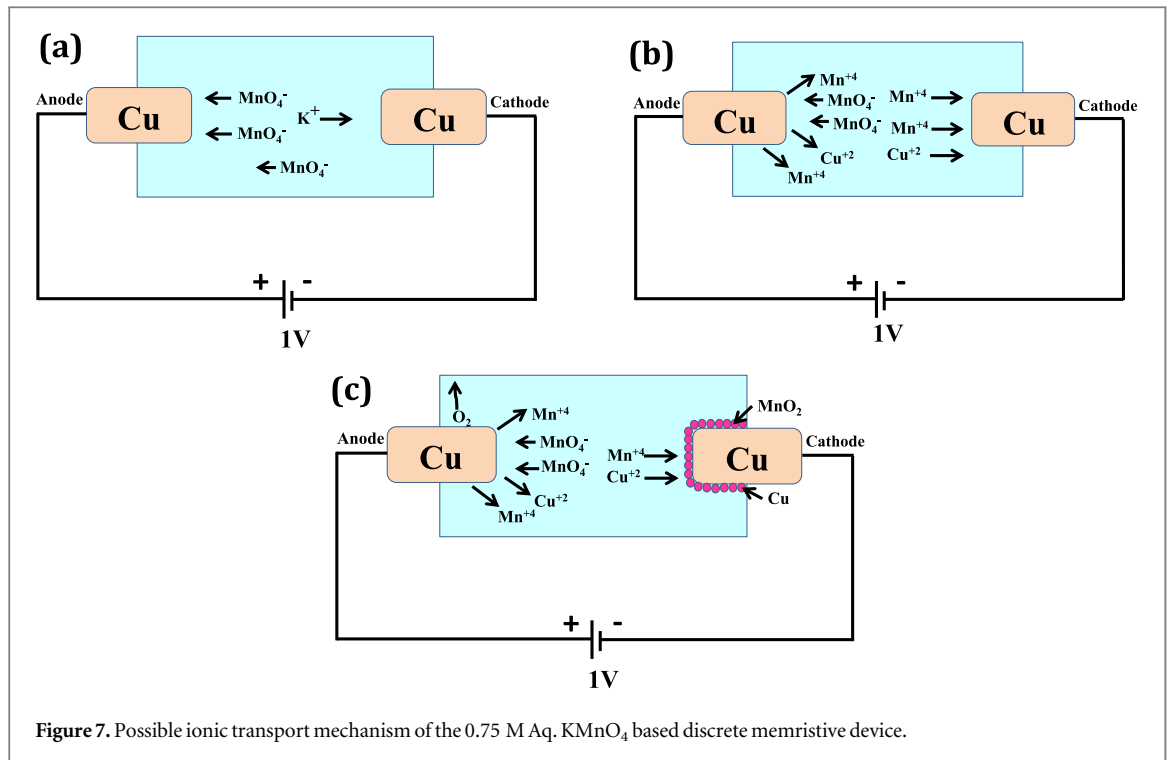
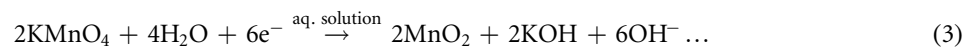


Figure 7. Possible ionic transport mechanism of the 0.75 M Aq. KMnO_4 based discrete memristive device.

Oxidation of $\text{Cu}_{(s)}$ due to KMnO_4 solution,



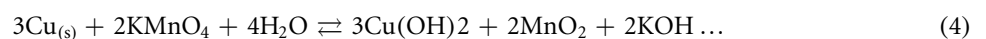
(Oxidation) (0.34 V)



(Reduction) (0.595 V)

During the reaction, the solution becomes basic ($\text{pH} = 8.15$) due to the formation of OH^- in the reduction reaction of aqueous KMnO_4 . The presence of MnO_2 was confirmed by pink color deposition on the cathode.

So, overall reaction at anode becomes,



Cathode: Cu electrode: Reduction

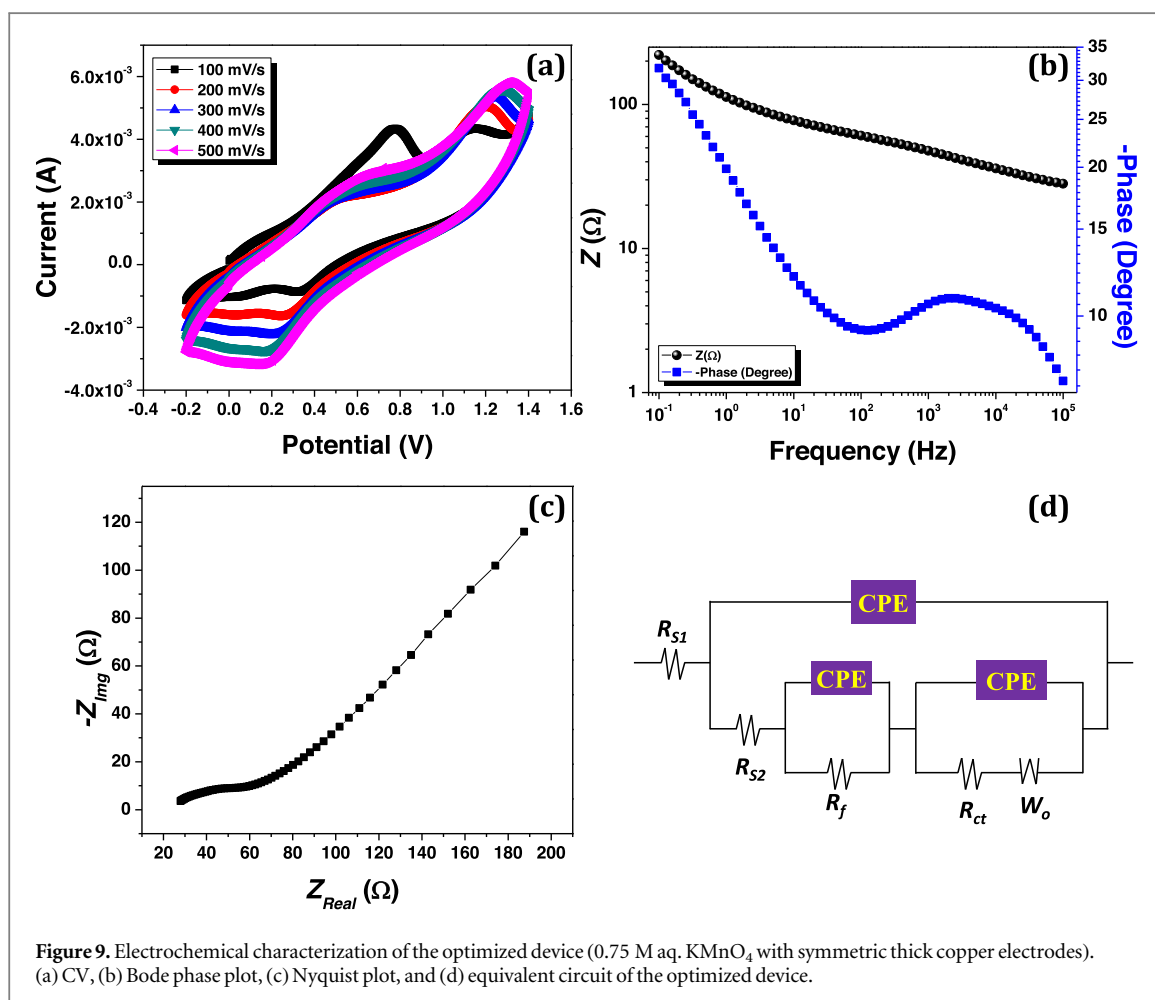
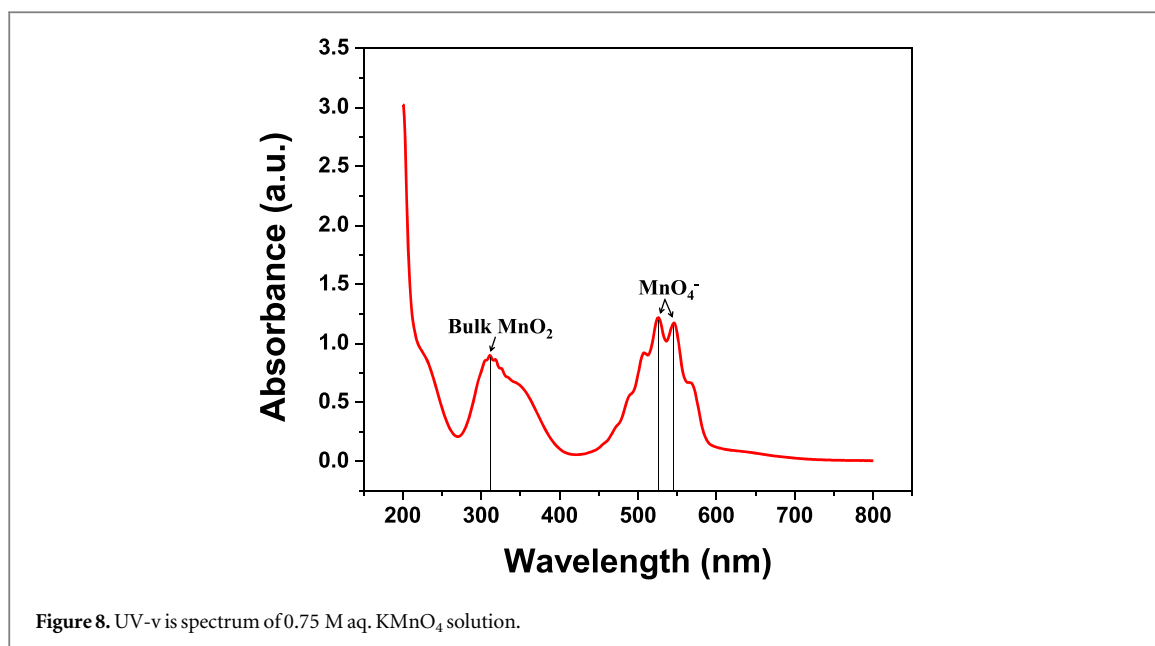


(reduction due to external voltage)

The Cu^{+2} ions produced due to oxidation of Cu electrode at the anode by applying external voltage get reduced at the cathode.

The proposed conduction mechanism was examined by the UV-visible absorption spectrum of aq. KMnO_4 . The UV-Visible absorption spectrum of aq. KMnO_4 solution (0.75 M) was recorded after the completion of the resistive switching process (figure 8). The spectrum shows absorption peaks at 310 nm (shoulder peak) [56]. Recently, Christopher *et al* have confirmed the presence of colloidal manganese (IV) peak around 300 nm [57]. The peaks related to manganese (IV) and MnO_2 are generally observed between 300–400 nm [58]. Furthermore, the bulk MnO_2 becomes MnO_2 nanoparticle nearly at 360 nm [59]. Therefore, the broad peak of bulk MnO_2 can be confirmed at 310 nm. The peaks at 525 nm and 545 nm confirm the presence of MnO_4^- in the solution [60]. The reaction mechanism and UV-Visible absorption spectrum results asserted that the RS of the present case was due to the ionic conduction of manganese and copper ions. We believe that further investigation and analysis are required in the case of the proposed conduction mechanism.

The electrochemical behavior of the aq. KMnO_4 (0.75 M) based discrete memristive device was studied using a potentiostat (Autolab electrochemical workstation) in the two-electrode configuration. In the present case, CV, bode phase plot, Nyquist plot, and equivalent circuit of the optimized device were obtained by using the electrochemical characterization method, as shown in figures 9(a) to (d), respectively. The K_2SO_4 with a molarity of 0.75 was added to the aq. KMnO_4 (0.75 M) solution, which acts as a supporting electrolyte in the present case. At the outset, the symmetric test cell with identical working and counter electrodes was used to investigate the CV of the optimized aq. KMnO_4 (0.75 M) based memristive device, as shown in figure 9(a). The CV



performance of the optimized memristive device was analyzed in the potential window of -0.2 V to 1.4 V, at varying scan rates ranging from 100 mV s^{-1} to 500 mV s^{-1} . An oxidation peak at 0.7 V was observed at the lower scan rate of 100 mV s^{-1} , which corresponds to the oxidation of Cu to Cu^+ . This peak was not observed for other increasing scan rates, which suggested that the Cu^+ state (which is less stable) had a very short leave, resulting in faster conversion to Cu^{2+} with good stability. The peak observed at 0.7 V corresponds to the +1 oxidation state of copper and this state is less stable as compared to the +2 state for copper. In the present case, the transition

from Cu^0 to Cu^{+2} is taking place. Transition to Cu^{+1} from Cu^0 requires lower oxidation potential, as compared to Cu^{+2} when it is considered on the standard scale having hydrogen as the reference. At lower scan rates, the peak will not disappear but will be seen more prominently. At lower scan rates, the rate of increase in potential allows enough time interval to attain an equilibrium state in which the +1 oxidation state of copper can survive. This condition of equilibrium will be more favored when we decrease the scan rate. On the other hand, at higher scan rates, there will not be enough time available for sustaining the +1 state to generate a peak and an instant transition from Cu^0 to Cu^{+2} is obtained, and no peak can be seen in the curve. The peak related to the Cu^{2+} can be seen more clearly, with further improvement in the scan rate. The peak at 1.14 V corresponds to the oxidation of Cu to Cu^{2+} . The reduction peak of Cu^{2+} was observed at 0.32 V (scan rate: 100 mV s^{-1}).

The Bode phase and Nyquist plots of 0.75 M aq. KMnO_4 with Cu:Cu symmetric thick electrodes are shown in figures 9(b) and (c), respectively. The Bode plot represents the frequency-dependent phase and impedance response of the discrete memristive device. The impedance of the device was high at a lower frequency and start to decreases for higher frequency. A similar trend was also observed for the phase angle property of the discrete memristive device. The Nyquist plot data was used to develop an equivalent circuit of the optimized memristive device, as shown in figure 9(d). Very low circuit fit error (0.3175%) was observed, therefore the equivalent circuit can provide a good realistic picture of the electrochemical kinetics of the aq. KMnO_4 based discrete memristive device. In the present case, the quasi-semicircle curve represents the electrolyte resistance (R_{S1}) and it was found to be 18.88Ω . The equivalent series resistance (R_{S2}) of the device, which is related to the combined internal electrode resistance and electrolyte resistance was found to be 2.73Ω [60]. The contact resistance (R_f) and charge transfer resistance (R_{ct}) were found to be 52.04Ω and 32.15Ω , respectively. The frequency-dependent slope line represents the Warburg ion diffusion resistance (W_O) which was found to be 0.005974Ω [61].

4. Conclusions

In conclusion, a facile way to fabricate a discrete memristive device was successfully demonstrated using aq. and methanol- KMnO_4 . The developed devices show typical hysteresis loop, bipolar memristive switching effect, and analog memory property at low SET (+1 V) and RESET (−1 V) voltages. In the case of the concentration optimization study, good memristive switching was achieved at a high concentration in aq. and methanol-based devices. The memristive hysteresis area and current magnitude were decreased as the concentration of aq. KMnO_4 decreases; however, nonlinearity was observed in the case of methanol- KMnO_4 based devices. All developed devices show the double valued charge-flux characteristics, suggesting that the aq. and methanol- KMnO_4 based devices are non-ideal memristors or memristive devices. The reliability study reveals that the 0.75 M aq. KMnO_4 based memristive device shows good endurance (10^3 cycles), satisfactory switching uniformity (coefficient of variation: < 12%), and excellent memory window (~ 124) during the cycle-to-cycle variation. The reaction mechanism and UV-visible absorption spectrum results asserted that the ionic conduction of manganese and copper ions was responsible for the memristive switching effect. Moreover, the enhancement of ion-pair dissociation in the aq. solution could be a possible reason for observed memristive switching. The reported low-cost and simple method may allow the fabrication of discrete memristive devices with enhanced electrochemical properties.

Acknowledgments

This research was supported by the MOTIE (Ministry of Trade, Industry & Energy (10080581)) and the KSRC (Korea Semiconductor Research Consortium) support program for the development of the future semiconductor device.

Data availability statement

All data that support the findings of this study are included within the article (and any supplementary files).

Conflict of interest

The authors declare that there is no conflict of interest.

ORCID iDs

Deok-kee Kim  <https://orcid.org/0000-0002-2515-4984>

Tukaram D Dongale  <https://orcid.org/0000-0003-2536-6132>

References

- [1] Chua L 1971 Memristor—the missing circuit element *IEEE Trans. Circuit Theory* **18** 507–19
- [2] Strukov D, Snider G, Stewart D and Williams R 2008 The missing memristor found *Nature* **453** 80–3
- [3] Schmitt R, Kubicek M, Sediva E, Trassin M, Weber M, Rossi A, Hutter H, Kreisel J, Fiebig M and Rupp J 2019 Accelerated ionic motion in amorphous memristor oxides for nonvolatile memories and neuromorphic computing *Adv. Funct. Mater.* **29** 1804782
- [4] Patil V, Patil A, Patil S, Khairnar N, Tarwal N, Vanalakar S, Bulakhe R, Patil P and Dongale T 2020 Bipolar resistive switching, synaptic plasticity and non-volatile memory effects in the solution-processed zinc oxide thin film *Mater. Sci. Semicond. Process.* **106** 104769
- [5] Xia Q and Yang J 2019 Memristive crossbar arrays for brain-inspired computing *Nat. Mater.* **18** 309–23
- [6] More S et al 2019 Resistive switching and synaptic properties modifications in gallium-doped zinc oxide memristive devices *Results Phys* **12** 1946–55
- [7] Vidiš M, Plecenik T, Moško M, Tomašec S, Roch T, Satrapinsky L, Grančič B and Plecenik A 2019 Gasistor: A memristor based gas-triggered switch and gas sensor with memory *Appl. Phys. Lett.* **115** 93504
- [8] Pawar A, Kanapally S, Kadam K, Patil S, Dongle V, Jadhav S, Kim S and Dongale T 2019 MemSens: a new detection method for heavy metals based on silver nanoparticle assisted memristive switching principle *J. Mater. Sci., Mater. Electron.* **30** 11383–94
- [9] Yongbin Y, Nijing Y, Chenyu Y and Tashi N 2019 Memristor bridge-based low pass filter for image processing *J Syst Eng Electron* **30** 448–55
- [10] Li C et al 2018 Analogue signal and image processing with large memristor crossbars *Nat. Electron.* **1** 52–9
- [11] Gale E 2015 Non-ideal memristors for a non-ideal world *Phys. Status Solidi A* **212** 229–38
- [12] Borghetti J, Snider G, Kuekes P, Yang J, Stewart D and Williams R 2010 Memristive switches enable stateful logic operations via material implication *Nature* **464** 873–6
- [13] Yang J, Strukov D and Stewart D 2013 Memristive devices for computing *Nat. Nanotechnol.* **8** 13–24
- [14] Huang H, Yang R, Tan Z, He H, Zhou W, Xiong J and Guo X 2019 Quasi-hodgkin–huxley neurons with leaky integrate-and-fire functions physically realized with memristive devices *Adv. Mater.* **31** 1803849
- [15] Zidan M, Strachan J and Lu W 2018 The future of electronics based on memristive systems *Nat. Electron.* **1** 22–9
- [16] Pawar K et al 2019 Highly reliable multilevel resistive switching in a nanoparticulated In₂O₃ thin-film memristive device *J Phys D: Appl Phy* **52** 175306
- [17] Dongale T et al 2018 Mimicking the biological synapse functions of analog memory, synaptic weights, and forgetting with ZnO-Based memristive devices *J. Nanosci. Nanotechnol.* **18** 7758–66
- [18] Das H, Xu Q and Datta P 2021 Effect of ZnS and PbS shell on mem-behavior of CdS quantum dots *J Mater Sci: Mater Electron* **32** 7049–60
- [19] Yoon K, Lee M, Kim G, Song S, Seok J, Han S, Yoon J, Kim K and Hwang C 2012 Memristive tri-stable resistive switching at ruptured conducting filaments of a Pt/TiO₂/Pt cell *Nanotechnology* **23** 185202
- [20] Lei Y, Liu Y, Xia Y, Gao X, Xu B, Wang S, Yin J and Liu Z 2014 Memristive learning and memory functions in polyvinyl alcohol polymer memristors *AIP Adv.* **4** 77105
- [21] Qin S, Dong R, Yan X and Du Q 2015 A reproducible write-(read) n-erase and multilevel bio-memristor based on DNA molecule *Org. Electron.* **22** 147–53
- [22] Rananavare A, Kadam S, Prabhu S, Chavan S, Anbhule P and Dongale T 2018 A reproducible write-(read) n-erase and multilevel bio-memristor based on DNA molecule *Mater. Lett.* **232** 99–102
- [23] Gurme S, Dongale T, Surwase S, Kumbhar S, More G, Patil V, Patil P, Kamat R and Jadhav P 2018 An Organic Bipolar Resistive Switching Memory Device Based on Natural Melanin Synthesized from *Aeromonas* sp. *SNS Phys. Status Solidi a* **215** 1800550
- [24] Yan K, Peng M, Yu X, Cai X, Chen S, Hu H, Chen B, Gao X, Dong B and Zou D 2016 High-performance perovskite memristor based on methyl ammonium lead halides *J. Mater. Chem. C* **4** 1375–81
- [25] Dongale T, Bagade A, Mohite S, Rananavare A, Orlowski M, Kamat R and Rajpuro K 2018 Bipolar resistive switching with coexistence of mem-elements in the spray deposited CoFe₂O₄ thin film *J. Mater. Sci., Mater. Electron.* **29** 3231–8
- [26] Gandhi G, Aggarwal V and Chua L 2013 The first radios were made using memristors *IEEE Circuits Syst. Mag.* **13** 8–16
- [27] Khanal G, Cardarilli G, Chakraborty A, Acciarito S, Mulla M, Di Nunzio L, Fazzolari R and Re M 2016 A ZnO-rGO composite thin film discrete memristor *IEEE Int Conf Semicond Electron Proc., ICSE* 129–32
- [28] Chew Z J and Li L, 2013 A discrete memristor made of ZnO nanowires synthesized on printed circuit board *J Mater. Lett.* **91** 298–300
- [29] Koo H-J, So J-H, Dickey M D and Veleo O D 2011 Towards all-soft matter circuits: Prototypes of quasi-liquid devices with memristor characteristics. *Adv. Mater.* **23** 3559–64
- [30] Merrikh-Bayat F and Parvizi M 2016 Practical method to make a discrete memristor based on the aqueous solution of copper sulfate *Appl Phys A: Mater Sci Process* **122** 602
- [31] Chougale M, Patil S, Shinde S, Khot S, Patil A, Khot A, Chougale S, Volos C, Kim S and Dongale T 2019 Memristive switching in ionic liquid-based two-terminal discrete devices *Ionics* **25** 5575–83
- [32] Kim D and Lee J 2019 Liquid-based memory and artificial synapse *Nanoscale* **11** 9726–32
- [33] Zhang P et al 2019 Nanochannel-Based transport in an interfacial memristor Can emulate the analog weight modulation of synapses *Nano Lett.* **19** 4279–86
- [34] Song J, Lee H, Wang Y and Wan C 2002 Two-and three-electrode impedance spectroscopy of lithium-ion batteries *J. Power Sources* **111** 255–67
- [35] Milano G, Porro S, Valov I and Ricciardi C 2019 Nanowire memristors: recent developments and perspectives for memristive devices based on metal oxide nanowires *Adv. Electron. Mater.* **5** 1970044
- [36] Adhikari S, Sah M, Kim H and Chua L 2013 Three fingerprints of memristor *IEEE Trans Circuits Syst I Regul Pap* **60** 3008–21
- [37] Dongle V, Dongare A, Mullani N, Pawar P, Patil P, Heo J, Park T and Dongale T 2018 Development of self-rectifying ZnO thin film resistive switching memory device using successive ionic layer adsorption and reaction method *J. Mater. Sci., Mater. Electron.* **29** 18733–41

- [38] Chua L 2011 Resistance switching memories are memristors *Appl Phys A: Mater Sci Process* **102** 765–83
- [39] Khot A, Desai N, Khot K, Salunkhe M, Chougule M, Bhavne T, Kamat R, Musselman K and Dongale T 2018 Bipolar resistive switching and memristive properties of hydrothermally synthesized TiO₂ nanorod array: Effect of growth temperature *Mater. Des.* **151** 37–47
- [40] Kim S, Han J, Kim H, Kim S and Jang H 2018 Recent Advances in Memristive Materials for Artificial Synapses *Adv. Mater. Technol.* **3** 1800457
- [41] Lee T, Hwang H, Woo J, Kim D, Kim T and Nahm S 2018 Synaptic Plasticity and Metaplasticity of Biological Synapse Realized in a KNbO₃ Memristor for Application to Artificial Synapse *ACS Appl. Mater. Interfaces* **10** 25673–82
- [42] Birolek Z, Birolek D, Birolekova V and Kolka Z 2015 Comments on Pinched Hysteresis Loops of Memristive Elements *Radioengineering* **24** 962–67
- [43] Dongale T et al 2018 Mimicking the synaptic weights and human forgetting curve using hydrothermally grown nanostructured CuO memristor device *J. Nanosci. Nanotechnol.* **18** 984–91
- [44] Valov I, Linn E, Tappertzhofen S, Schmelzer S, van den Hurk J, Lentz F and Waser R 2013 Nanobatteries in redox-based resistive switches require extension of memristor theory *Nat. Commun.* **4** 1–9
- [45] Saraf S, Markovich M, Vincent T, Rechter R and Rothschild A 2013 Memory diodes with nonzero crossing *Appl. Phys. Lett.* **102** 022902
- [46] Tappertzhofen S, Linn E, Böttger U, Waser R and Valov I 2013 Nanobattery effect in RRAMs—implications on device stability and endurance *IEEE Electron Device Lett.* **35** 208–10
- [47] Shuai Y, Du N, Ou X, Luo W, Zhou S, Schmidt O and Schmidt H 2013 Improved retention of nonvolatile bipolar BiFeO₃ resistive memories validated by memristance measurements *Phys. Status Solidi C* **10** 636–9
- [48] Patil S, Chougale M, Rane T, Khot S, Patil A, Bagal O, Jadhav S, Sheikh A, Kim S and Dongale T 2018 Solution-processable ZnO thin film memristive device for resistive random-access memory application *Electronics* **7** 445
- [49] Liu M, Borowiec J, Sun L, Konop M, Rahman M, Taallah A, Boi F and Gillin W 2019 Experimental studies on the conduction mechanism and electrical properties of the inverted Ba doped ZnO nanoparticles based memristor *Appl. Phys. Lett.* **115** 73505
- [50] Gul F 2018 Carrier transport mechanism and bipolar resistive switching behavior of a nano-scale thin film TiO₂ memristor *Ceram. Int.* **44** 11417–23
- [51] Du N, Shuai Y, Luo W, Mayr C, Schüffny R, Schmidt O and Schmidt H 2013 Practical guide for validated memristance measurements *Rev. Sci. Instrum.* **84** 023903
- [52] Sarkar P, Bhattacharjee S, Barman A, Kanjilal A and Roy A 2016 Multilevel programming in Cu/NiO_y/NiO_x/Pt unipolar resistive switching devices *Nanotechnology* **27** 435701
- [53] Bousoulas P and Tsoukalas D 2016 Understanding the formation of conducting filaments in RRAM Through the design of experiments *Int. J. High Speed Electron. Syst.* **25** 1640007
- [54] Wang T, Meng J, He Z, Chen L, Zhu H, Sun Q, Ding S and Zhang D 2019 Atomic layer deposited Hf_{0.5}Zr_{0.5}O₂-based flexible memristor with Short/Long-Term synaptic plasticity *Nanoscale Res. Lett.* **14** 102
- [55] Dongale T et al 2017 Effect of write voltage and frequency on the reliability aspects of memristor-based RRAM *Int Nano Lett* **7** 209–16
- [56] Ede S, Anantharaj S, Nithiyantham U and Kundu S 2015 DNA-encapsulated chain and wire-like β-MnO₂ organosol for oxidative polymerization of pyrrole to polypyrrole *Phys. Chem. Chem. Phys.* **17** 5474–84
- [57] Hindson C, Francis P, Hanson G, Adcock J and Barnett N 2010 Mechanism of permanganate chemiluminescence *Anal. Chem.* **82** 4174–80
- [58] Kim H, Watthanaphanit A and Saito N 2016 Synthesis of colloidal MnO₂ with a sheet-like structure by one-pot plasma discharge in permanganate aqueous solution *RSC Adv.* **6** 2826–34
- [59] Jaganyi D, Altaf M and Wekesa I 2013 Synthesis and characterization of whisker-shaped MnO₂ nanostructure at room temperature *Appl. Nanosci.* **3** 329–33
- [60] Thesing A, Loguercio L, NoreMBERG B, Alano J, Silva R, Orlandi M, Marin G, Santos J and Carreño N 2019 Carreño, Tunable graphene oxide inter-sheet distance to obtain graphene oxide-silver nanoparticle hybrids *New J. Chem.* **43** 1285–90
- [61] Zhang R, Bao J, Wang Y and Sun C 2019 Concentrated electrolytes stabilize bismuth-potassium batteries *Chem. Sci.* **9** 6193–8